Electromagnetic absorption of circularly polarized ultrasound in tungsten in the region of the Doppler-shifted cyclotron resonance

V. V. Gudkov and I. V. Zhevstovskikh

Institute of Metal Physics, Ural Scientific Center of the Academy of Sciences of the USSR, Sverdlovsk
(Submitted 13 June (1986)
Zh. Eksp. Teor. Fiz. **92**, 208–220 (January 1987)

The absorption of circularly polarized ultrasonic waves was investigated experimentally in tungsten as a function of the magnetic field **H**. It was found that, at frequencies above 100 MHz, the main doppleron-phonon resonance peak, observed for negative polarization, was accompanied in weaker fields, corresponding to the region of cyclotron absorption, by two additional absorption peaks, one of which had the same polarization and the other a different (+) polarization. Phenomenological theories are used to show that the additional peaks can be described by field coupling between elastic and electronic subsystems of the metal. Quantitative data are obtained on the positions of the peaks as functions of the magnetic field axis, and on their halfwidths. These data can be used to determine the off-diagonal (Hall) components of the nonlocal conductivity tensor $\hat{\sigma}$, both beyond the cyclotron absorption edge and in the region of cyclotron absorption. Moreover, the diagonal (transverse to **H**) components of $\hat{\sigma}$ can also be found beyond the cyclotron absorption edge.

INTRODUCTION

Absorption of ultrasound in pure metals at low temperatures is largely determined by the interaction between the elastic subsystem and conduction electrons. When an external magnetic field is present, this interaction exhibits resonance. For $\mathbf{k}\|\mathbf{H}$, $|\mathbf{k}|l \gg 1$, and $\Omega\tau \gg 1$, there are observable singularities due to the Doppler-shifted cyclotron resonance (DSCR) of conduction electrons when $\omega < \Omega \lesssim \mathbf{k}\cdot\bar{\mathbf{v}}$ ($\mathbf{k}$ and ω are, respectively, the wave vector and frequency of the ultrasonic waves; Ω, l, and $\bar{\mathbf{v}}$ are, respectively, the cyclotron frequency, mean free path, and carrier velocity averaged over the cyclotron period; and τ is the relaxation time of the distribution function). These singularities are responsible for deformational absorption peaks[1] and the doppleron-phonon resonance (DPR)[2] that appears for $\mathbf{k}\cdot\bar{\mathbf{v}} < \Omega$ but is due to DSCR.[3]

DPR in tungsten was discovered and investigated by the authors of Ref. 4, but no account was taken of the fact that the eigenmodes involved in the propagation of the ultrasonic waves along a high symmetry axis (at least a threefold axis) were circularly polarized waves, and that the resonance manifested itself differently in different circular polarizations. This gave rise to ellipticity and the rotation of the plane of polarization of the initially linearly polarized ultrasonic waves,[5,6] and hence to a distortion of the line shape. These effects masked some of the singularities and shifted the resonance maximum on the absorption curve recorded by measuring the signal amplitude at the receiver input when the sensitive directions of the receiving and transmitting piezotransducers were parallel.

In this paper, we report a study of the absorption of circularly polarized ultrasonic waves in tungsten. By extracting the circularly polarized components from the signal reaching the receiving piezotransducer, we were able to detect new features in the cyclotron absorption region,[7] to determine the absorption line halfwidth, and to measure more accurately the resonance field in the DPR region. These experimental results were used as a basis for a method of determining the diagonal components of the nonlocal conductivity tensor beyond the cyclotron absorption edge, and to extend the method of reconstructing the off-diagonal (Hall) components described in Ref. 8 to the cyclotron absorption region.

THEORY

Under the conditions of resonant interaction between the elastic and electronic subsystems of a metal, the eigenmodes are the coupled elastoelectromagnetic and electromagnetoelastic waves transporting the energy of the electromagnetic field and of the elastic oscillations. When the coupling between the elastic and electronic subsystems is weak (the criterion for this is that the change in the wave vectors of eigenmodes in the region of resonance is small), one of these energies predominates. In the absence of generally agreed terminology, we shall speak of *elastic modes* when elastic oscillations predominate and *ultrasonic modes* when the relevant frequency range is considered.

Experiment confirms[5] that there is weak coupling under DPR in tungsten. For wave propagating along the z-axis parallel to the magnetic field $\mathbf{H} = (0,0,H)$, which is also the direction of a fourfold rotational symmetry axis, the solution of the dispersion relation (see, for example, Ref. 9) can be written in the following form to first order in the coupling coefficient:

$$k^{(\pm)} = k_0\left[1 - \frac{i\omega\alpha^{(\pm)} + H^2/4\pi}{2\lambda_{1313}} - \frac{k_0^2}{2\rho\omega}\,\frac{(\beta^{(\pm)} \pm icHk_0/4\pi\omega)^2}{c^2k_0^2/4\pi\omega + i\sigma^{(\pm)}}\right], \tag{1}$$

where $k^{(\pm)}$ are the z-components of the complex wave vectors of the circularly polarized ultrasonic waves, ρ is the density of the metal, λ_{1313} is the component of the quasistatic tensor of elastic moduli for $H = 0$, c is the velocity of light, $k_0 = \omega/s_0$, and s_0 is the velocity of transverse ultrasound for $H = 0$. The quantities $\alpha^{(\pm)} = \alpha_{1313} \pm i\alpha_{1323}$, $\sigma^{(\pm)} = \sigma_{11} \pm i\sigma_{21}$, and $\beta^{(\pm)} = \beta_{113} \pm i\beta_{123}$, which are functions of k_0 and H, are the Fourier components of the tensor α characterizing the elasticity of the electron gas, the conductivity tensor $\hat{\sigma}$, and the tensor $\hat{\beta}$ which represents the "deforma-

 0038-5646/87/010117-07$04.00

tional" conductivity and the "electromagnetic" elasticity of the electron gas:

$$\alpha_{ijkl}=\langle\Lambda_{ij},\ \Lambda_{kl}\rangle, \tag{2}$$

$$\beta_{ijk}=e\langle\Lambda_{ij},\ v_k\rangle, \tag{3}$$

$$\sigma_{ij}=e^2\langle v_i,\ v_j\rangle, \tag{4}$$

where Λ_{ij} are the components of the deformational potential tensor, whose average over the Fermi surface is zero, v_i are the components of the carrier velocity, and $e<0$ is the electron charge. When the transport equation is solved in the relaxation time approximation, we have, for arbitrary a and b,

$$\langle a, b\rangle = \frac{4\pi}{h^3}\int\limits_{\Pi\Phi} dp_z |m_c| \sum_{n=-\infty}^{\infty} \frac{(a)_n (b)_n^*}{R_n}, \tag{5}$$

$$(a)_n = \frac{1}{2\pi}\int\limits_0^{2\pi} d\theta a(\theta)\exp\left\{-\frac{i}{\Omega}\int\limits_0^{\theta} d\theta_1[\mathbf{k}\cdot(\mathbf{v}(\theta_1)-\bar{\mathbf{v}})+n\Omega]\right\}, \tag{6}$$

$$R_n=\tau^{-1}-i(\mathbf{k}\cdot\mathbf{v}-\omega-n\Omega), \tag{7}$$

where $\Omega = -eH/cm_c$, h is Planck's constant, and p and m_c are, respectively, the crystal momentum and cyclotron mass. When the Fermi surface consists of several sheets, the right-hand sides of (2)–(4) are sums of integrals corresponding to the individual sheets.

The second term in brackets in (1) is due to the deformational interaction, and the third to the field (electromagnetic) interaction between the elastic and electronic subsystems of the metal. The first term describes the manifestations of DPR.

EXPERIMENT

In our experiment, we used cylindrical tungsten samples (W-1 and W-2) of diameter $d\simeq 10$ mm and length respectively equal to 4.57 mm and 2.89 mm. The resistivity ratio was $\rho_{300}/\rho_{4.2\ K}\gtrsim 1.5\times 10^5$. The samples were produced in the Crystallization Laboratory of the Metal Physics Institute of the Ural Science Center of the USSR Academy of Sciences. The transverse ultrasonic waves were generated and detected by x-cut lithium niobate piezotransducers. The direction of propagation and the magnetic field both lay along the [001] crystal axis. The measurements were performed at $T=4.2$ and 1.8 K in the frequency range 64–262 MHz, using a pulsed phase-sensitive system based on the principle of the frequency-tunable acoustic bridge.[10]

The method used to determine the absorption of circularly polarized elastic waves as a function of the magnetic field is described in Ref. 11. It involves measurement of the amplitude $\Delta N_j = \ln[(A_j(H)-A_j(0))/A_j(0)]$, where A_j is the signal amplitude at the receiver, and the phase $\Delta\varphi_j = \varphi_j(H)=\varphi_j(0)$ of the signal for parallel ($j=1$) and antiparallel ($j=2$) propagation relative to the field vector **H**. The receiving and transmitting piezotransducers used to detect and generate linearly polarized oscillations are arranged at an angle $\psi\neq n\pi/2 (n=0,\ \pm 1,\ \pm 2, \ldots)$ in the plane perpendicular to the wave vector. It can be shown that, in the case of traveling waves, $\Delta k^{(\pm)} = k^{(\pm)}(H)-k^{(\pm)}(0)$ is given by

$$\Delta k^{(\pm)} = \frac{1}{il}\ln\{(\exp[\Delta N_2+i(\Delta\varphi_2\pm\psi)] - \exp[\Delta N_1+i(\Delta\varphi_1\mp\psi)])[i2\sin(\pm\psi)]^{-1}\}, \tag{8}$$

where l is the acoustic path length. This expression was obtained on the assumption that the elastic oscillations at the receiving piezotransducer were the result of the interference between two circularly polarized waves, labeled (+) and (−), that had equal amplitudes and group velocities for $H=0$. Moreover,

$$|[s^{(\pm)}(H)-s_0]/s_0|\ll 1, \tag{9}$$

where $s^{(\pm)}(H)$ are the phase velocities of the circularly polarized eleastic waves. We note that (9) is a condition for the validity of the weak-coupling approximation.

Figure 1 shows the measured absorption of circularly polarized ultrasonic waves, $\Delta\Gamma^{(\pm)} = \Gamma^{(\pm)}(H) - \Gamma^{(\pm)}(0) = -\operatorname{Im}\Delta k^{(\pm)}$, in the DPR region. It is clear that, for frequencies $f\gtrsim 100$ MHz ($f=\omega/2\pi$), the resonance corresponding to the (−) polarization appears in the form of two peaks, namely, a principal peak and a subsidiary peak (the

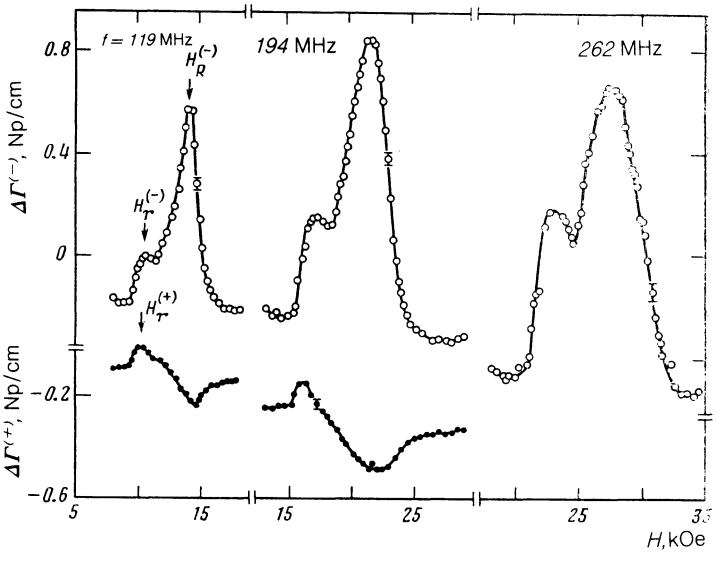

FIG. 1. Absorption of circularly polarized ultrasonic waves as a function of the applied magnetic field at $T=4.2$ K.

resonance fields at $f = 119$ MHz are denoted by $H_R^{(-)}$ and $H_r^{(-)}$, respectively). The subsidiary peak does not appear at lower frequencies (cf. Fig. 1 of Ref. 5). In the (+) polarization, an antiresonance feature is observed in the region of the principal maximum and there is a small peak at $H = H_r^{(+)}$ (we shall also refer to it as a subsidiary peak).

INTERPRETATION OF ABSORPTION PEAKS

To elucidate the nature of the absorption peaks, we must turn to model descriptions. We shall consider the electron sheet of the Fermi surface in the form of a slab section of a sphere[8] (the sphere radius $p_1 = 0.268\times10^8\hbar$ g·cm·s^{-1} is equal to the measured radius,[12] and the radius of the base section is $p_0 = 0.179\times10^8\hbar$ g·cm·s^{-1}), whereas the hole sheet will be taken in the form of a cylinder of the same volume. For this model, the components σ_{21} and σ_{11} of the nonlocal conductivity tensor are shown in Fig. 2 as functions of the magnetic field. We know that the real part of the denominator of the field term in (1) vanishes at the ultrasound absorption maximum in the DPR region:

$$k_0^2c^2/4\pi\omega - (\operatorname{sign} P)\sigma_{21}(k_0, H) = 0, \qquad (10)$$

with sign $P = \pm 1$ for the two polarizations ($\pm$), respectively. The solution of (10) can be obtained graphically by determining the intersection of the curve $\sigma_{21}(k_0, H)$ and the straight lines $\pm k_0^2c^2/4\pi\omega$. Figure 2 shows that this intersection occurs in a field $H_R^{(-)}$, where

$$|\sigma_{21}/\sigma_{11}| \gg 1. \qquad (11)$$

This is a condition for the solution of the dispersion equation that corresponds to a weakly-damped electromagnetic mode, i.e., a doppleron, where $k_0 = \operatorname{Re} k_D$ for $H = H_R^{(-)}$ (k_D is the z-component of the doppleron wave vector), i.e., we are dealing with a doppleron-phonon resonance. Moreover, the intersection of the $\sigma_{21}(k_0,H)$ curve and the straight lines $\pm k_0^2c^2/4\pi\omega$ will also occur in the region of cyclotron absorption ($H < H_1$, where H_1 corresponds to DSCR for electrons with maximum $|m_c v_z|$). The fact that the real part of the denominator, in the field term vanishes in the region of cyclotron absorption leads to an increase in the electromagnetic absorption of ultrasond, which can appear in the form of resonance peaks under certain conditions (which we shall analyze below).

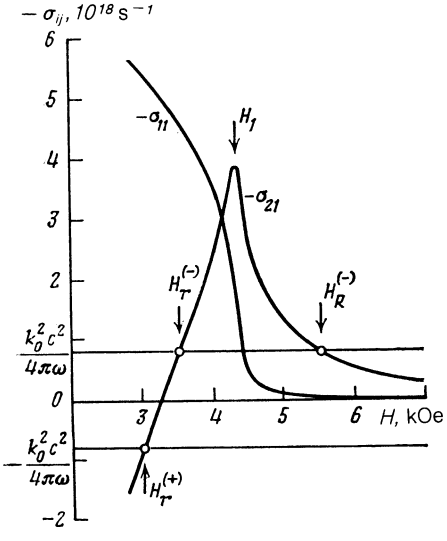

FIG. 2. Components of the nonlocal conductivity tensor as functions of the magnetic field for a model Fermi surface and $k_0 = 2\pi f/s_0$, $f = 150$ MHz, $s_0 = 2.88\times10^5$ cm/s, $\tau = 5\times10^{-9}$ s.

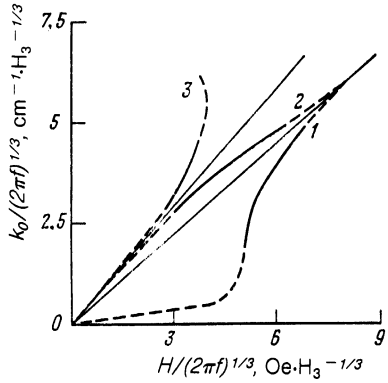

FIG. 3. Relationship between k_0 and the magnetic field satisfying (10) for σ_{21} (k_0,H) and the model Fermi surface. Curve 1—(−) polarization, $H > H_1$; curve 2—(−) polarization, $H < H_1$; curve 3—(+) polarization, $H < H_1$.

The relation between the real component of the ultrasound wave vector and the resonance value of the field can be represented by the curves shown in Fig. 3. It is clear that these curves differ from the linear plots typical for the deformational absorption peaks. For long wavelengths, the positions of the electromagnetic absorption peaks tend asymptotically to a single line passing through the origin (similarly to curves 2 and 3 in Fig. 3), whereas, in the short-wavelength region, they depart from this asymptote, and the peak position curve for the (−) polarization tends to the DPR absorption curve at a point lying on the $k_0v_z = \Omega$ line, as shown by curves 2 and 1 of Fig. 3.

Figure 4 shows the experimental results for the principal peak (DPR) and the subsidiary peaks. These curves are similar to the calculated curves in Fig. 3. The quantitative discrepancy in the magnetic field values is explained by the fact that, in this model, the value $|m_c v_z|$, which is typical for the resonance electrons in a real metal, is not reached. It is

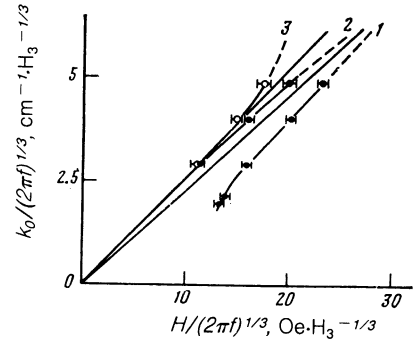

FIG. 4. Relationship between k_0 and the resonance value of the magnetic field for tungsten. Curve 1—(−) polarization, principal resonance; curve 2—(−) polarization, subsidiary resonance; curve 3—(+) polarization, subsidiary resonance.

also important to note that the expeirmental curves are recorded in a limited range of frequency and magnetic field. This is so because the size of the absorption peaks is proportional to the square of the frequency, so that the peaks have a much lower amplitude as the frequency is reduced, and are then difficult to measure. On the other hand, as the frequency increases, all the resonant features shift toward stronger magnetic fields, at which there are quantum oscillations in absorption, which also impedes determinations of peak position along the magnetic field axis. Analysis of the relationships shown in Figs. 3 and 4 can thus be used to interpret the experimentally recorded subsidiary peaks as being due to the electromagnetic absorption of ultrasound in the DSCR region.

All the resonances features can be arbitrarily divided into spatial, temporal, and wave resonances. Spatial and temporal resonances arise under the conditions of spatial or temporal dispersion when the wavelength λ and frequency ω of the ultrasonic wave are comparable with the characteristic length L_i or frequency ω_i of the electron subsystem:

$$\lambda = L_i, \quad \omega = \omega_i. \tag{12}$$

Wave resonances are observed when the spatial distribution of elastic fields at a given frequency that is produced by the ultrasonic wave is the same at the structure of the fields corresponding to the eigenmodes of the electronic subsystem. The formal criterion for wave resonance is

$$\operatorname{Re} \mathbf{k}^{(P)}(\omega) = \operatorname{Re} \mathbf{k}_e^{(P)}(\omega), \tag{13}$$

where $\mathbf{k}^{(P)}$ and $\mathbf{k}_e^{(P)}$ are the wave vectors of the ultrasonic wave and of some eigenmode of the electronic subsystem of polarization P, respectively.

Despite the fact that the presence of the subsidiary peaks is related to spatial dispersion, the above classification forces us to treat them as quasi-spatial resonances: Eq. (12) with L_i replaced with u_p (the displacement electrons in one cyclotron period) is satisfied only approximately. For example, (12) is satisfied to within 10% in the case of the subsidiary resonance in the (−) polarization.

In their appearance and formal description the subsidiary peaks are analogous to DPR, but they are observed when an atypical (for dopplerons) relationship holds between the components of the conductivity tensor: $|\sigma_{11}| \gtrsim |\sigma_{21}|$. Since the existence of both DPR and the subsidiary peaks is due to the fact that the nonlocal Hall conductivity has an extremum-type singularity due to the DSCR of a group of carriers, the additional peaks are referred to as "satellites." These satellites seem to be relatively common for metals in which DPR is observed. They are essentially pseudo-DPR phenomena because the value of k_0 for which the real part of the denominator of the field term vanishes for $H = H_r^{(\pm)}$ is not a solution of the dispersion equation corresponding to a weakly-damped electromagnetic mode (in contrast to true DPR).

DETERMINATION OF NONLOCAL CONDUCTIVITY

The circular components of the nonlocal conductivity tensor will now be written in the form

$$\sigma^{(\pm)}(k_0, H) = i\sigma_0[\pm F'(q, \gamma) + iF''(q, \gamma)]. \tag{14}$$

The functions F' and F'' are real and determine the nondissipative (σ_{21}) and dissipative (σ_{11}) components of the tensor $\hat{\sigma}$; $\sigma_0 = n_e|e|c/H$ is the static electron hall conductivity; $n_e = n_h$ is the density of electrons (and holes); and $\gamma = 1/\Omega_p \tau_p$ (the index p characterizes, and will do so below, the resonance electrons). The nonlocal parameters defined by

$$q = \frac{k_0 c}{2\pi |e| H} \left(\frac{\partial S}{\partial p_z} \right)_p,$$

where S is the area bounded by the cyclotron orbit in **p**-space. The nonlocal parameter is numerically equal to the ratio of the displacement of resonant carriers in one cyclotron period and the wavelength.

When the nonlocal conducitivity is determined from the DPR data,[8] it is usual to neglect the dependence of F' and F'' on γ, assuming that the collision-free limit has been reached. Our experiments have shown that the resonance singularity in $\Gamma^{(-)}(H)$ increases as the temperature is reduced from 4.2 to 1.8 K. This shows that, at least for the components $\sigma^{(\pm)}$ and $\beta^{(\pm)}$, the collision-free limit had not been reached, and the γ dependence of the nonlocal conductivity cannot be neglected. This means that the function F' deduced from experimental data (we shall represent it by F_s') will be a curve on the surface $F' = F'(q,\gamma)$. To find F_s', it is sufficient to transform (10) in the light of (14), so that

$$F_s' = (\operatorname{sign} P) cf H_R^{(-)} / 2 s_0^2 n_e |e|. \tag{15}$$

The value of the nonlocal parameter for which F_s' is given by (15) is

$$q = \omega \theta^{-1} / s_0 H_R^{(-)}, \tag{16}$$

where θ^{-1} is the slope of the asymptote $k_0(v_z)_p = \Omega_p$ of the curve representing the position of DPR as a function of the magnetic field in the short-wavelength region. In the $(H/\omega^{1/3}, k_0/\omega^{1/3})$ plane, this is given by

$$\theta^{-1} = \frac{c}{2\pi |e|} \left(\frac{\partial S}{\partial p_z} \right)_p = \frac{c}{|e|} (m_c v_z)_p.$$

Since the determination of the nonlocal conductivity from DPR data is based on the use of (10), which is also valid for fields corresponding to the positions of the satellite, we have the possibility of extending the method used to determine F' to the DSCR region. Formulas (15) and (16) then remain valid provded $H_R^{(-)}$ is replaced with $H_r^{(\pm)}$.

Figures 5a and b show projections of the curves $F' = F_s'(q,\gamma)$ onto the $\gamma = \text{const}$ and $F' = \text{const}$ planes for $\theta^{-1} = 4.42$ Oe·cm. The broken line in Fig. 5a in the region $q < 0.6$ is drawn with allowance for the fact that, for a charge-neutralized metal,

$$\lim_{q \to 0,\ \gamma \neq 0} F'(q, \gamma) = 0.$$

Since, for finite τ, the conductivity is finite even at $q = 1$, the $F_s'(q,\gamma)$ curve reaches an extremum at this point. If we suppose that, above 262 MHz, the projection of $F_s'(q,\gamma)$ onto the $F' = \text{const}$ plane is as shown by the broken line in Fig. 5b, we can estimate the extremal value of F_s' at room temperature, which turns out to be $(F_s')_{\text{extr}} \simeq 0.42$. The broken line corresponding to $0.94 < q < 1.05$ in Fig. 5a is drawn using this value of $(F_s')_{\text{extr}}$.

We now turn to the determination of $(F_s'')(q,\gamma)$, which requires an analysis of the magnetic field dependence of the components $\alpha^{(\pm)}$ and $\beta^{(\pm)}$. In an anisotropic metal, the contributions of the individual sheets of the Fermi surface to

$\alpha^{(\pm)}$ and $\beta^{(\pm)}$ are resonant in character in the region of cyclotron absorption. The resonances may partially overlap and thus complicate the analysis of the experimental data. However, in our case, we have a simplifying circumstance: DPR in tungsten is due to the electrons with the largest value of $|m_c v_z|$. According to Ref. 8, these electrons lie near the base point of the spheroid, which is shaped like a toy "jack." As a result, when the absorption curve is analyzed, the contribution of the hole sheets of the Fermi surface to $\alpha^{(\pm)}$ and $\beta^{(\pm)}$ can be taken in the strong field limit $k_0 v_z \ll \Omega$ (local limit), while the electron contribution will have a dependence similar to that of $\sigma^{(\pm)}$ because all these tensor components [cf. (2)–(7)] are determined by integrals of the same form, and differ only in the numerators of the integrands (which contain smoothly-varying functions), and the resonant singularities of these tensor components are due to the common denominator R_n. As far as the contribution of the hole sheets to $\alpha^{(\pm)}$ and $\beta^{(\pm)}$ is concerned, it is shown in Ref. 13 that the only nonzero components are those of $\alpha^{(\pm)}$, where, for fixed k_0, the quantities $\mathrm{Re}\,\alpha^{(\pm)}$ in the expression for $\Gamma^{(\pm)}$ do not depend on H. Thus, if we isolate the contribution of the resonance electrons to the absorption coefficient $\Delta\Gamma_p^{(\pm)} = \Gamma^{(\pm)}(H) - \Gamma_\infty^{(\pm)}$, where $\Gamma_\infty^{(\pm)}$ is the value of $\Gamma^{(\pm)}$ for $H \gg H_1$, then, beyond the cyclotron absorption edge, the quantitiy $\Delta\Gamma_p^{(\pm)}$ will be given by

$$\Delta\Gamma_p^{(\pm)} = \frac{k_0^3}{2\rho\omega}\sigma_{11}\left(\mathrm{Im}\,\beta^{(\pm)} \pm \frac{cHk_0}{4\pi\omega}\right)^2 \times \left[\sigma_{11}^2 + \left(\frac{c^2k_0^2}{4\pi\omega} \mp \sigma_{21}\right)^2\right]^{-1}. \quad (17)$$

Let us denote by ΔH the width of the high-field wing of the absorption line at half-heigth, and let us write out the expression for $\Delta\Gamma_p^{(-)}$ in the field $H_\Delta = H_R^{(-)} + \Delta H$, normalized to the value $\Delta\Gamma_p^{(-)}(H_R^{(-)})$, and transfer to the left-hand side the terms containing σ_{11}. The result is

$$[2B^2\sigma_{11}(k_0, H_R^{(-)}) - \sigma_{11}(k_0, H_\Delta)]\sigma_{11}(k_0, H_\Delta) = [\sigma_{21}(k_0, H_\Delta) - \sigma_{21}(k_0, H_R^{(-)})]^2,$$

$$B^2 = \left[\mathrm{Im}\,\beta^{(-)}(k_0, H_\Delta) - \frac{cH_\Delta k_0}{4\pi\omega}\right]^2 \times \left[\mathrm{Im}\,\beta^{(-)}(k_0, H_R^{(-)}) - \frac{cH_R^{(-)}k_0}{4\pi\omega}\right]^{-2}. \quad (18)$$

It is clear from (17) that the reduction in $\Delta\Gamma_p^{(-)}$ for $H > H_R^{(-)}$ is due to the reduction in the numerator of the field term and an increase in the difference $k_0^2c^2/4\pi\omega - |\sigma_{21}|$. When the last factor predominates and the dependence of σ_{11} on H is weak, which occurs, for example, for the above model (see Fig. 2), then, for narrow resonances (in tungsten, $\Delta H/H_R^{(-)}$ is less than 5%), we have

$$B^2 \approx 1, \quad \sigma_{11}(k_0, H_\Delta) \approx \sigma_{11}(k_0, H_R^{(-)}). \quad (19)$$

Equation (18) then becomes

$$[\sigma_{11}(k_0, H_\Delta)]^2 \approx [\sigma_{21}(k_0, H_\Delta) - \sigma_{21}(k_0, H_R^{(-)})]^2. \quad (20)$$

When we determine the function $\sigma_{21}(k_0, H_\Delta)$ in (20), we shall neglect the dependence of F' on γ within the line half-width. In practice, this means that we shall use the projection of the experimental curve $F_s'(q,\gamma)$ onto the $\gamma = \mathrm{const}$ plane. As in the case of the real component of the function $F(q,\gamma)$, the graphical representation of the imaginary term is the surface $F'' = F''(q,\gamma)$ in three-dimensional space, and the DPR data can be used to determine only the curve $F'' = F_s''(q,\gamma)$ on the surface. We note that the projections of the experimental curves $F' = F_s'(q,\gamma)$ and $F'' = F_s''(q,\gamma)$ onto the q, γ plane are somewhat different, since F_s' is determined from the position of the absorption peak, whereas F_s'' is determined form the field corresponding to the width of the high-field wing, i.e., $F_s' = F_s'(q_R, \gamma_R)$ and $F_s'' = F_s''(q_\Delta, \gamma_\Delta)$, where the subscripts of q and γ are the same as those of H for which the corresponding values of q and γ are determined. Transforming to the components of the normalized nonlocal conductivity in (20), we obtain

$$F_s''(q_\Delta, \gamma_\Delta) \approx F_s'(q_\Delta) - (H_\Delta/H_R^{(-)})F_s'(q_R). \quad (21)$$

The projection of the $F'' = F_s''(q,\gamma)$ curve onto the $\gamma = \mathrm{const}$ plane is shown in Fig. 5c for $q < 1$. The expression given by (21) was obtained using the approximation defined by (19), so that the values of F_s'' must be regarded as very approximate.

The half-width of the resonance line in the region of cyclotron absorption depends on a larger number of factors as compared with the area beyond the cyclotron absorption edge, so that even a very approximate estimate cannot be obtained in this region for $F''(q,\gamma)$.

DISCUSSION

Let us now compare the procedures used to determine the nonlocal conductivity by the radiofrequency size effect method[8] (RSEM) with the DPR method.

In the case of RSEM, $F'(q)$ is determined from the dopplerons dispersion curves. The dependence of $\mathrm{Re}\,k_D$ on H for $\omega = \mathrm{const}$ is found from the surface impedance oscillations due to the excitation of dopplerons. The condition that the oscillations will be observed is that the imaginary component of the doppleron wave vector be small in comparison with the real part:

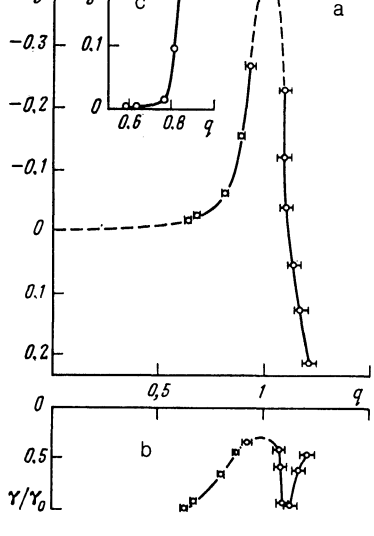

FIG. 5. Projections of $F_s'(q,\gamma)$ onto the $\gamma = \mathrm{const}$ plane (a) and of $F' = \mathrm{const}$ (b) and $F_s''(q,\gamma)$ onto the $\gamma = \mathrm{const}$ plane (c), determined experimentally for tungsten.

$$|\mathrm{Im}\, k_D/\mathrm{Re}\, k_D| \ll 1,$$

which is satisfied if

$$|\sigma_{11}/\sigma_{21}| = |F''/F'| \ll 1. \tag{22}$$

It would appear that the same condition should apply to the DPR method: substantial damping of the doppleron should cause the resonance in ultrasound absorption to vanish. However, this is not so. Let us analyze the conditions ensuring that the relative half-width of the absorption line be small under DPR conditions, $\Delta H/H_R^{(-)} \ll 1$. This analysis can be done by substituting in (20) the linear expansion for $\sigma_{21}(k_0, H_\Delta)$ in terms of H at $H = H_R^{(-)}$. We then have

$$[\sigma_{11}(k_0, H_\Delta)]^2 \approx [\Delta H (\partial\sigma_{21}/\partial H)_{H=H_R^{(-)}}]^2.$$

The last term in the derivative

$$\frac{\partial\sigma_{21}}{\partial H} = -\frac{\sigma_0}{H}\left[F' + q\frac{\partial F'}{\partial q} + \gamma\frac{\partial F'}{\partial \gamma}\right]$$

can be neglected for $|\gamma| \ll 1$. The results is

$$\frac{\Delta H}{H_R^{(-)}} \approx \left|\frac{\sigma_{11}(k_0, H_\Delta)}{H_R^{(-)}(\partial\sigma_{21}/\partial H)_{H=H_R^{(-)}}}\right| \approx \left|\frac{(H_R^{(-)}/H_\Delta)\, F''(q_\Delta, \gamma_\Delta)}{F'(q_R, \gamma_R) + q_R (\partial F'/\partial q)_{q=q_R,\, \gamma=\gamma_R}}\right|. \tag{23}$$

This expression shows that the half-width of the absorption line is proportional to the dissipative component of the conductivity F''. This is as expected. However, if we recall condition (22), what is unexpected is that the denominator of (22) contains not only F', but also its derivative with respect to q, which ensures that the width of the relative absorption line half-width is sufficiently small even when F'' is of the same order as or exceeds F'. This is due to the fact that the denominator on the right-hand side of (23) indicates how rapdily $\sigma_{21}(k_0, H)$ and the straight line $k_0^2 c^2/4\pi\omega$ approach the resonance region in Fig. 2. The first term in the denominator on the right-hand side of (23) describes the variation in σ_{21} due to the static Hall conductiviity (it is present even in the case of the helicon-phonon resonance), and the second is due to nonlocal effects. We thus see why a well-defined ultrasound absorption maximum is observed for $q > 0.8$ in tungsten, despite the fact that F' and F'' are of the same order: the change in the conductivity due to nonlocal effect is quite large in this region.

A qualitatively similar discussion can be given for the satellites. Their existence can be explained by the fact that $\partial F'/\partial q$ is so large in their region that resonances can appear even when an inequality given by (22) is reversed. It is interesting to note that the presence of the derivative $\partial F'/\partial q$ in (23) can cause not only narrowing of the resonance peak, but also broadening when $F' \simeq -q_R \partial F'/\partial q$. This means that the $\sigma_{21}(k_0, H)$ curve and the straight line $k_0^2 c^2/4\pi\omega$ intersect at a small angle.

It follows from the foregoing discussion that the field interaction between the elastic and electronic subsystems of the metal can give rise to resonances on the absorption curve for circularly polarized ultrasound. Narrow electromagnetic absorption peaks are observed when

$$\left|F''\Big/\left(F' + q\frac{\partial F'}{\partial q}\right)\right| \ll 1.$$

If (22) is satisfied at the same time, we have a wave resonance. Measurements of the nonlocal conductivity in tungsten have shown that (22) is then a weak inequality, and the doppleron absorption is strong. The consequence of this is that a resonance occurring beyond the cyclotron absorption edge must be regarded as a quasi-wave resonance.

We now turn to the question as to whether it is necessary to extract the circularly polarized components from the signal reaching the detecting piezotransducer. If we suppose that the resonance is observed in one of the circular polarizations, while there is no change in absorption in the other component, it would seem that the usual method will suffice to determine the line half-width and the position of the resonance peak, i.e., the circular components need not be separated out. This is valid, at any rate, when the rotation of the plane of polarization is small. However, one cannot guarantee in advance that polarization phenomena will be absent or small. Measurements performed on tungsten have shown that, for $f \lesssim 100$ MHz, the rotation of the plane of polarization is small for ultrasound path lengths $l \lesssim 1$ cm (see Fig. 2 of Ref. 5). At higher frequencies, the polarization phenomena can no longer be neglected. To confirm this, in Fig. 6 we show the rotation of the plane of polarization ϕ and ellipticity ε at 194 MHz for $l = 0.29$ cm. To establish which polarization phenomena are responsible for the distortion of the ultrasound absorption curves obtained by the usual method, we can use the curves of Fig. 7, which show the apparent absorption $\Delta N_a = N_a(H) - N_a(0)$ and the absorption of the circularly polarized resonance mode $\Delta N^{(-)} = 20\Delta\Gamma^{(-)} l \times \log e$. The word, "apparent," was introduced in Ref. 14 in relation to the curve obtained by measuring the signal ampli-

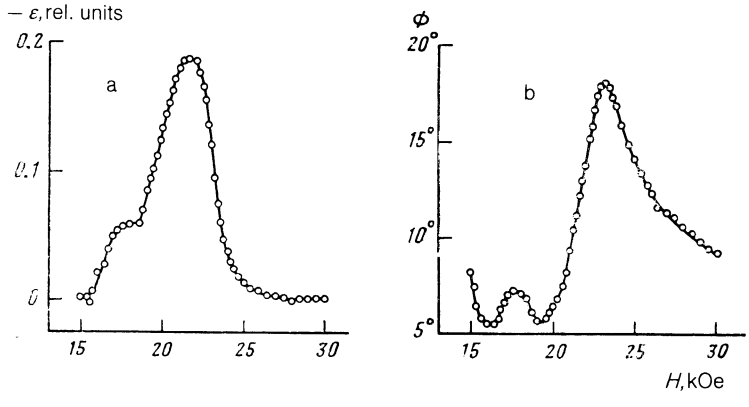

FIG. 6. Ellipticity ε (a) and angle of rotation of the plane of polarization ϕ (b) for ultrasound in tungsten. Frequency 194 MHz, acoustic path length 0.29 cm.

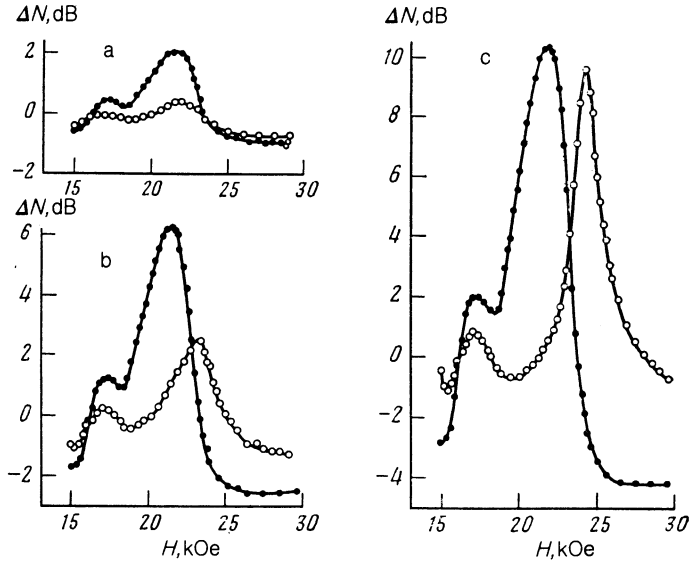

FIG. 7. "Apparent" absorption ΔN_a (open circles) and absorption $\Delta N^{(-)}$ of waves with (−) polarization (full points) as functions of magnetic field for ultrasound path length $l = (2n-1)L$, where $L = 0.29$ cm is the speciment length; a—$n = 1$, b—$n = 2$, c—$n = 3$.

tude at the receiver input for the parallel orientation of the sensitive directions of the receiving and transmitting piezotransducers. The dependence of N_a on H was calculated from the following expressions:

$$\Delta N_a = -20 \lg \{(A_1^2 + A_2^2)^{1/2}/2\},$$
$$A_1 = \exp(-\Delta k^{(+)\prime\prime} l)\cos(\Delta k^{(+)\prime} l) + \exp(-\Delta k^{(-)\prime\prime} l)\cos(\Delta k^{(-)\prime} l),$$
$$A_2 = \exp(-\Delta k^{(+)\prime\prime} l)\sin(\Delta k^{(+)\prime} l) + \exp(-\Delta k^{(-)\prime\prime} l)\sin(\Delta k^{(-)\prime} l),$$

where $\Delta k^{(\pm)} = \Delta k^{(\pm)\prime} + i\Delta k^{(\pm)\prime\prime}$ are determined from (8). It is clear from Fig. 7 that the functions $\Delta N_a(H)$ are significantly different from $\Delta N^{(-)}(H)$ and, as the path traversed by the waves increases, there is a change not only in the shape of the apparent absorption curve, but also in the position of the peak as a function of the magnetic field. It follows that the shortest possible samples have to be used to determine the position of the principal resonance and the half-width of the ultrasound absorption line in tungsten, and the circular components of the received signal must be isolated. As far as the satellites are concerned, they are found to merge into a single peak when the circular components are not separated.

CONCLUSIONS

Our main conclusions may be summarized as follows.

1. It is shown experimentally that DSCR for electrons with the maximum value of $|m_c v_z|$ in tungsten takes the form of a quasi-wave doppleron-phonon resonance in the (−) polarization and two quasi-spatial resonances (pseudo-DPR) in different circular polarizations.

2. These resonances are due to the field coupling between the elastic subsystem and the conduction electrons, which appears in the form of a principal peak and two satellites on the absorption curves for circularly polarized ultrasonic waves.

3. It is shown that the presence of well-resolved ultrasound field absorption peaks is due to a relationship between σ_{11} and the magnitude of $H(\partial\sigma_{21}/\partial H)$, and not between σ_{11} and σ_{21}, which determines the existence of a weakly-damped electromagnetic mode, namely, a doppleron.

4. Qualitative data on the half-width and position of the field absorption peaks for circularly polarized ultrasonic waves can be used to estimate the diagonal components of the nonlocal conductivity tensor of a metal beyond the cyclotron absorption edge, and to find the off-diagonal components, not only beyond the edge, but also in the region of cyclotron absorption.

The authors are indebted to R. Sh. Nasyrov for supplying them with the tungsten specimens used in the experiments.

[1]S. W. Hui and J. A. Rayne, J. Phys. Chem. Solids **33**, 611 (1972).
[2]L. T. Tsymbal and T. F. Butenko, Solid State Commun. **13**, 633 (1973).
[3]S. V. Medvedev, V. G. Skobov, L. N. Fisher, and V. A. Yudin, Zh. Eksp. Teor. Fiz. **69**, 2267 (1975).
[4]A. A. Galkin, L. T. Tsymbal, T. F. Butenko, A. N. Cherkasov, and A. M. Grishin, Phys. Lett. A **67**, 207 (1978).
[5]K. B. Vlasov and V. V. Gudkov, Fiz. Met. Metalloved. **46**, 892 (1978).
[6]K. B. Vlasov and V. V. Gudkov, Pis'ma Zh. Eksp. Teor. Fiz. **28**, 516 (1978) [JETP Lett. **28**, 479 (1978)].
[7]V. V. Gudkov and I. V. Zhevstovskikh, Pis'ma Zh. Eksp. Teor. Fiz. **43**, 582 (1986) [JETP Lett. in press].
[8]T. F. Butenko, V. T. Vitchinkin, A. A. Galkin, *et al.*, Zh. Eksp. Teor. Fiz. **78**, 1811 (1980) [Sov. Phys. JETP **51**, 909 (1980)].
[9]J. Mertching, Phys. Status Solidi **37**, 465 (1970).
[10]E. A. Masalitin, V. D. Fil', and P. M. Gorborukov, Izmeritel'naya Tekh. **11**, 69 (1979).
[11]V. V. Gudkov and K. B. Vlasov, Fiz. Met. Metalloved. **46**, 254 (1978).
[12]V. V. Boĭko and V. A. Gasparov, Zh. Eksp. Teor. Fiz. **61**, 2362 (1971) [Sov. Phys. JETP **34**, 1266 (1972)].
[13]K. B. Vlasov, A. B. Rinkevich, and A. M. Burkhanov, Fiz. Met. Metalloved. **53**, 295 (1982).
[14]J. R. Boyd and J. D. Gavenda, Phys. Rev. **152**, 645 (1966).

Translated by S. Chomet